2-16-2011

First IBEX observations of the terrestrial plasma sheet and a possible disconnection event

D. J. McComas

M. A. Dayeh

H. O. Funsten

S. A. Fuselier

J. Goldstein

See next page for additional authors

First IBEX observations of the terrestrial plasma sheet and a possible disconnection event

D. J. McComas,[1,2] M. A. Dayeh,[1] H. O. Funsten,[3] S. A. Fuselier,[4] J. Goldstein,[1,2] J.-M. Jahn,[1,2] P. Janzen,[5] D. G. Mitchell,[6] S. M. Petrinec,[4] D. B. Reisenfeld,[5] and N. A. Schwadron[1,7]

Received 21 September 2010; revised 23 November 2010; accepted 21 December 2010; published 16 February 2011.

[1] The Interstellar Boundary Explorer (IBEX) mission has recently provided the first all-sky maps of energetic neutral atoms (ENAs) emitted from the edge of the heliosphere as well as the first observations of ENAs from the Moon and from the magnetosheath stagnation region at the nose of the magnetosphere. This study provides the first IBEX images of the ENA emissions from the nightside magnetosphere and plasma sheet. We show images from two IBEX orbits: one that displays typical plasma sheet emissions, which correlate reasonably well with a model magnetic field, and a second that shows a significant intensification that may indicate a near-Earth (~10 R_E behind the Earth) disconnection event. IBEX observations from ~0.5–6 keV indicate the simultaneous addition of both a hot (several keV) and colder (~700 eV) component during the intensification; if IBEX directly observed magnetic reconnection in the magnetotail, the hot component may signify the plasma energization.

Citation: McComas, D. J., et al. (2011), First IBEX observations of the terrestrial plasma sheet and a possible disconnection event, *J. Geophys. Res.*, *116*, A02211, doi:10.1029/2010JA016138.

1. Introduction

[2] Energetic neutral atoms (ENAs) emitted from the Earth's magnetosphere are energetic ions that neutralize by charge exchange with the cold (few eV) neutral atoms in the geocorona, which surrounds the Earth. Since the original serendipitous observations of energetic neutral atoms (ENAs) emanating from the Earth's magnetosphere over two decades ago [*Roelof*, 1987], ENA observations have become increasingly important for understanding the global magnetospheric system. These observations have included limited high-energy ENA images from the Polar spacecraft [e.g., *Henderson et al.*, 1997] and broad energy coverage observations from the Imager for Magnetopause-to-Aurora Global Exploration (IMAGE) mission [*Burch*, 2000]. IMAGE flew largely during geomagnetically active times from 2000 to 2005, and the bulk of its ENA studies focused on magnetosphere dynamics, including magnetospheric substorms [*Pollock et al.*, 2003, and references therein] and storms [e.g., *Pollock et al.*, 2001; *Brandt et al.*, 2002; *McComas et al.*, 2002; *Skoug et al.*, 2003; *Perez et al.*, 2004a, 2004b; *DeMajistre et al.*, 2004; *Henderson et al.*, 2006; *Zaniewski et al.*, 2006].

[3] In contrast to the single point observations from IMAGE, the Two Wide-angle Imaging Neutral-atom Spectrometers (TWINS) mission [*McComas et al.*, 2009a] began making stereo ENA images of the magnetosphere in June 2008; these observations have continued through the deepest solar minimum of the space age. In spite of the geomagnetically quiet times, TWINS observations are contributing importantly to the understanding of small storms (minimum Dst ~ −70) [*Valek et al.*, 2010] and bright low-altitude emissions, which paint precipitating ring current ion fluxes onto the Earth's upper atmosphere [e.g., *Bazell et al.*, 2010]. Simultaneous TWINS observations from widely separated vantage points have allowed inversion of the magnetospheric ion distributions, which were able to reasonably reproduce in situ ion observations measured by THEMIS, both in terms of magnitude and the observed multipeaked radial profile [*Grimes et al.*, 2010; J. D. Perez et al., Validation of a method for obtaining ion intensities from ENA images using data from TWINS and THEMIS, submitted to *Journal of Geophysical Research*, 2011]. Perez et al. (submitted manuscript, 2011) further showed that these observations can be inverted to provide accurate pitch angle distributions over the entire ring current spatial distribution. The complementary analysis technique of forward modeling from the dual TWINS vantage points was recently applied to a weak storm from 2008, producing global ion distributions whose modeled ENA images agree

[1]Southwest Research Institute, San Antonio, Texas, USA.
[2]Department of Physics and Astronomy, University of Texas at San Antonio, San Antonio, Texas, USA.
[3]Los Alamos National Laboratory, Los Alamos, New Mexico, USA.
[4]Lockheed Martin Advanced Technology Center, Palo Alto, California, USA.
[5]Department of Physics and Astronomy, University of Montana, Missoula, Montana, USA.
[6]Johns Hopkins University Applied Physics Laboratory, Laurel, Maryland, USA.
[7]Department of Physics, University of New Hampshire, Durham, New Hampshire, USA.

0148-0227/11/2010JA016138

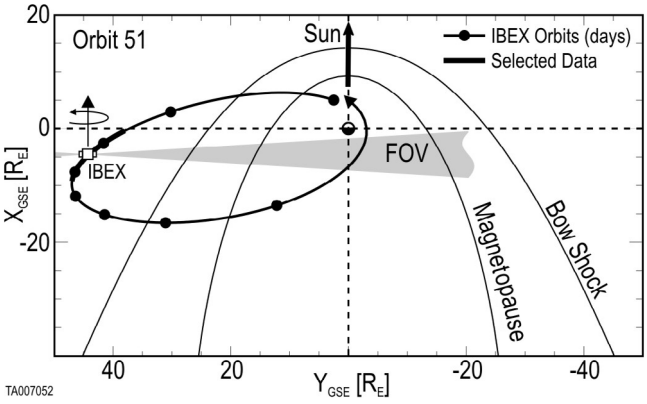

Figure 1. Diagram of IBEX Orbit 51 which extends from 27 October 2009 to 2 November 2009. IBEX's highly elliptical and near-ecliptic orbit provides nearly ideal viewing of vertical cuts (gray FOV) through the magnetosphere and plasma sheet from the side. The thicker "selected data" portion of the orbit is used to generate the image in Figure 3.

with TWINS to within about 20% (P. C. Brandt et al., Simultaneous TWINS and THEMIS observations of the spatial, spectral and pitch angle ion distributions of the ring current, submitted to *Journal of Geophysical Research*, 2011). TWINS observations have also been especially suitable for comparison to global magnetospheric modeling because TWINS provides essentially continuous global coverage throughout entire storm events with periodic stereo viewing intervals. For example, *Buzulukova et al.* [2010] used the Comprehensive Ring Current Model in combination with TWINS data to explain weak storm postmidnight enhancements. As valuable as the dual vantage point stereo imaging from TWINS is for unfolding magnetospheric ENA images of the inner magnetosphere, these generally nadir viewing measurements are taken from near the Earth (<8 R_E), where obliquely viewing the tenuous plasma sheet down the tail is very difficult.

[4] The extent and structure of the geocorona are critical to quantitatively understanding magnetospheric ENA emissions. The most recent analyses of the geocorona used new observations from the Ly-α detectors [*Nass et al.*, 2006] on TWINS [*McComas et al.*, 2009a]. *Zoennchen et al.* [2010] inverted Ly-α line of sight intensities to reconstruct the three-dimensional density structure of the hydrogen geocorona at geocentric distances from 3 to 7 R_E during the recent quiet solar conditions. These authors found hydrogen densities consistent with previous results [*Hodges*, 1994; *Rairden et al.*, 1986; *Østgaard et al.*, 2003] close to the Earth, but higher densities at >3.5 R_E and an antisunward enhancement indicating an extended hydrogen "geotail."

[5] In contrast to the "bright" low-altitude emissions and routinely observable ring current emissions, this study examines dim ENA emissions from the more distant plasma sheet, where the geocorona is extremely tenuous. *McComas et al.* [2002] provided the first ENA observations of the extended plasma sheet as a function of distance down the magnetotail using observations from the Medium Energy Neutral Atom (MENA) imager on IMAGE in a high-latitude nearly polar Earth orbit (apogee ~8 R_E). These authors focused on enhanced emissions during two large magnetospheric storms and needed to integrate ENAs from across the entire tail width in order to produce adequate statistics. Nonetheless, these authors demonstrated that ENA emissions can be observed to several tens of R_E deep in the magnetotail and that enhanced emissions (high densities in the distant plasma sheet) are associated with high densities both in the solar wind and plasma sheet at geosynchronous orbit. Using the same viewing from IMAGE [*Scime et al.*, 2002] and then TWINS [*Keesee et al.*, 2011, generated average energy spectra from many days worth of viewing to produce average ion temperature maps of the deeper magnetotail. Finally, *Brandt et al.* [2002] examined 10–60 keV plasma sheet and ring current emissions using data from the IMAGE High Energy Neutral Atom (HENA) imager. These authors integrated all ENAs from ~8–14 R_E and across the entire tail to find rapid decreases in integrated ENA fluxes around the time of magnetic dipolarizations, which were followed within 10–20 min by ion injections at geosynchronous orbit. These authors also found larger than expected plasma sheet ENA fluxes and suggested that exospheric densities on the nightside may be enhanced over symmetric models of the geocorona, consistent with the recent, direct observations from TWINS [*Zoennchen et al.*, 2010].

[6] The Interstellar Boundary Explorer (IBEX) mission (see *McComas et al.* [2009b] and other papers in the IBEX Special Issue of Space Science Reviews) was launched 19 October 2008. IBEX has already provided the first global observations and maps of the heliosphere's interstellar interaction [*McComas et al.*, 2009c; *Fuselier et al.*, 2009; *Funsten et al.*, 2009a; *Schwadron et al.*, 2009], first direct observations of interstellar H and O drifting in from the local interstellar medium [*Möbius et al.*, 2009], first observations of ENAs from the Moon [*McComas et al.*, 2009d] and first images of the Earth's subsolar magnetosheath [*Fuselier et al.*, 2010]. In this study we show the first images of the terrestrial plasma sheet and magnetotail using data from IBEX. In contrast to IMAGE and TWINS, IBEX views the magnetotail largely from the side and from outside the magnetosphere. Furthermore, IBEX's huge sensitivity allows spatially and temporally resolved ENA measurements of the very low ENA fluxes from the distant tail.

2. Observations

[7] The IBEX spacecraft rotates at ~4 RPM with its spin axis pointed roughly toward the Sun. Figure 1 shows the geometry for Orbit 51, data from which is analyzed in detail later in the paper. At the start of each ~7.5 day orbit, near perigee, the spin axis is pointed slightly west of the Sun (~1.5°). Because the spacecraft is in Earth orbit, its inertially fixed spin axis appears to drift eastward, across the Sun, and ends ~6° east of the Sun by the next perigee and repointing maneuver. The IBEX-Hi and –Lo sensors view perpendicular to the spin axis, collecting ENAs as a function of spin angle. This configuration provides extremely high-sensitivity ENA observations of each ~7° wide (FWHM) swath of the sky every six months [*McComas et al.*, 2009b].

[8] In contrast to heliospheric observations, viewing of the magnetosphere is driven by the fact that the magnetosphere is always aligned with the sunward direction (actually aberrated ~5° by the Earth's orbital motion compared to the solar wind), so in an Earth-based reference frame,

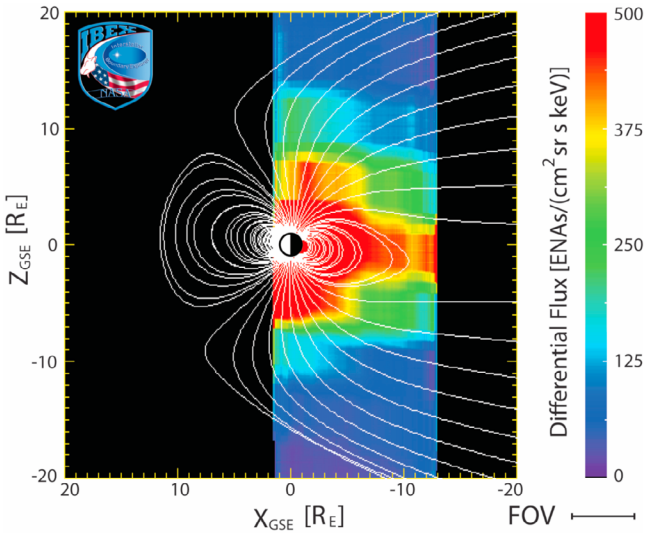

Figure 2. Differential fluxes of observed ENAs projected onto the GSE X-Z plane. This image shows time-averaged ENA fluxes in IBEX-Hi energy step 5 (2.0–3.8 keV FWHM) from 1048 UT on 5 November 2009 to 0223 UT on 7 November 2009. Note that the instantaneous FOV of IBEX is ~5.5 R_E wide (lower right corner), so the image was built up as IBEX's viewing moved slowly down the tail. Field lines were generated with the CCMC Tsyganenko model for the central time of the data interval covered.

IBEX's orbital axis appears to rotate around the Earth by 360° each year. During the winter, IBEX's apogee is sunward of the Earth and it does not view the magnetosphere except close to perigee; in the summer, IBEX is embedded in the magnetosphere and magnetotail throughout its orbit. However, twice per year, IBEX moves around the flanks of the magnetosphere on successive orbits and provides excellent viewing of various regions of the magnetosphere. In the spring of each year IBEX views the magnetosphere from the dawn side, while in the fall it views the magnetosphere from the dusk side, as shown in Figure 1. In these orbits, IBEX's viewing perpendicular to its nearly Sun-pointed spin axis provides continuous cuts through the magnetosphere with comparatively slow variations in position as the spacecraft moves along its orbit (e.g., the thicker "selected data" portion of this orbit is nearly 2 days). The IBEX sensors' field of view (FOV) is ±3.5°FWHM, so from a position ~45 R_E to the side (Y), the FOV instantaneously views a swath ~5.5 R_E wide in downtail (Z) distance, and integrates ENAs arriving from everywhere within this region. The more distant viewing of the plasma sheet from the side provides an excellent geometry to look for variations in the location and thickness of the plasma sheet generally, and thinning and disconnection events, in particular.

[9] Figure 2 shows a view of the magnetosphere and plasma sheet in ENAs from IBEX; this image was produced with data from Orbit 52, which is nearly identical to Orbit 51, but rotated ~7° clockwise from that shown in Figure 1. Geomagnetic activity was extremely quiet over Orbit 52, so it provides a good example of ENA emissions from the expected quiet time configuration of the magnetosphere. Both ENA images shown in this paper are from IBEX-Hi energy step 5 with a central energy of 2.7 keV (2.0–3.8 keV FWHM), and use triple coincidence measurements, which have extremely low backgrounds [*Funsten et al.*, 2009b]. The ENA emissions shown in Figure 2 are line of sight integrated measurements of the convolution of the magnetospheric ion flux and geocoronal neutral density. Nonetheless, they clearly "paint out" the densest portions of the plasma sheet, largely following the modeled magnetic structure. Images in other IBEX energy passbands are similar and also follow the expected magnetic structure.

[10] The magnetospheric ENA emissions, and thus ion density, show enhancements from the ring current region inside ~6 R_E; emissions from this region are also bright because the geocoronal density (and thus neutrals available for charge exchange) drops off with distance from the Earth, so ENAs are preferentially emitted from closer distances within the IBEX FOV. In the tail, the brighter emissions generally follow the superposed magnetic field model with the greatest enhancements in the plasma sheet region, which generally fills the central portion of the tail [e.g., *Slavin et al.*, 1985; *Mukai et al.*, 1996]. Regions of little emission along the top and bottom of the tail in this image are the low-density lobes, which are "open" or magnetically connected to both the Earth and the solar wind. The cross-tail current sheet and plasma sheet appears to be several R_E thick, consistent with statistical studies of in situ plasma and field observations [e.g., *Kaufmann et al.*, 2001]. In addition, the plasma sheet can appear thicker in ENA images for several reasons. First, because the image comprises ENAs generated at various positions across the plasma sheet it averages over source regions that vary significantly as a function of Y_{GSE}. Also, because of the offset of the Earth's

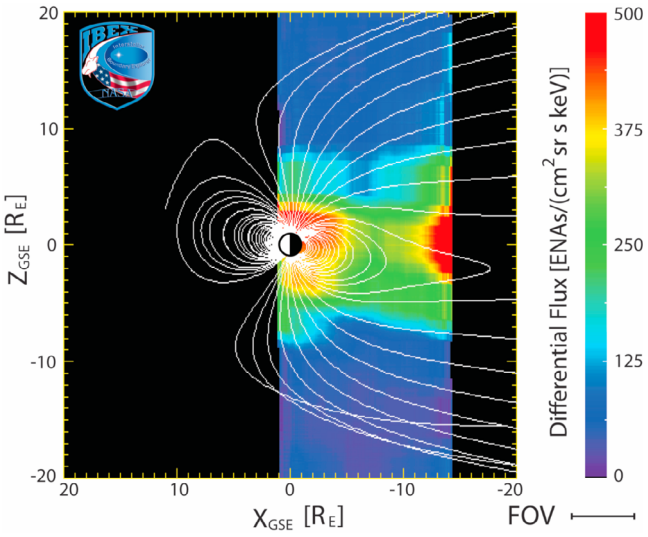

Figure 3. IBEX ENA image of a possible disconnection event at ~1020 UT on 29 October 2009, using ENAs in the same energy range and the same projection and color bar as in Figure 2. It is important to note that neither Figure 3 nor Figure 2 are snapshots but instead integrate ENA fluxes as IBEX's viewing swath (FWHM viewing width shown in lower right corner) moved slowly down the tail: in Figure 3 averaging fluxes from 2121 UT on 27 October 2009 to 1340 UT on 29 October 2009.

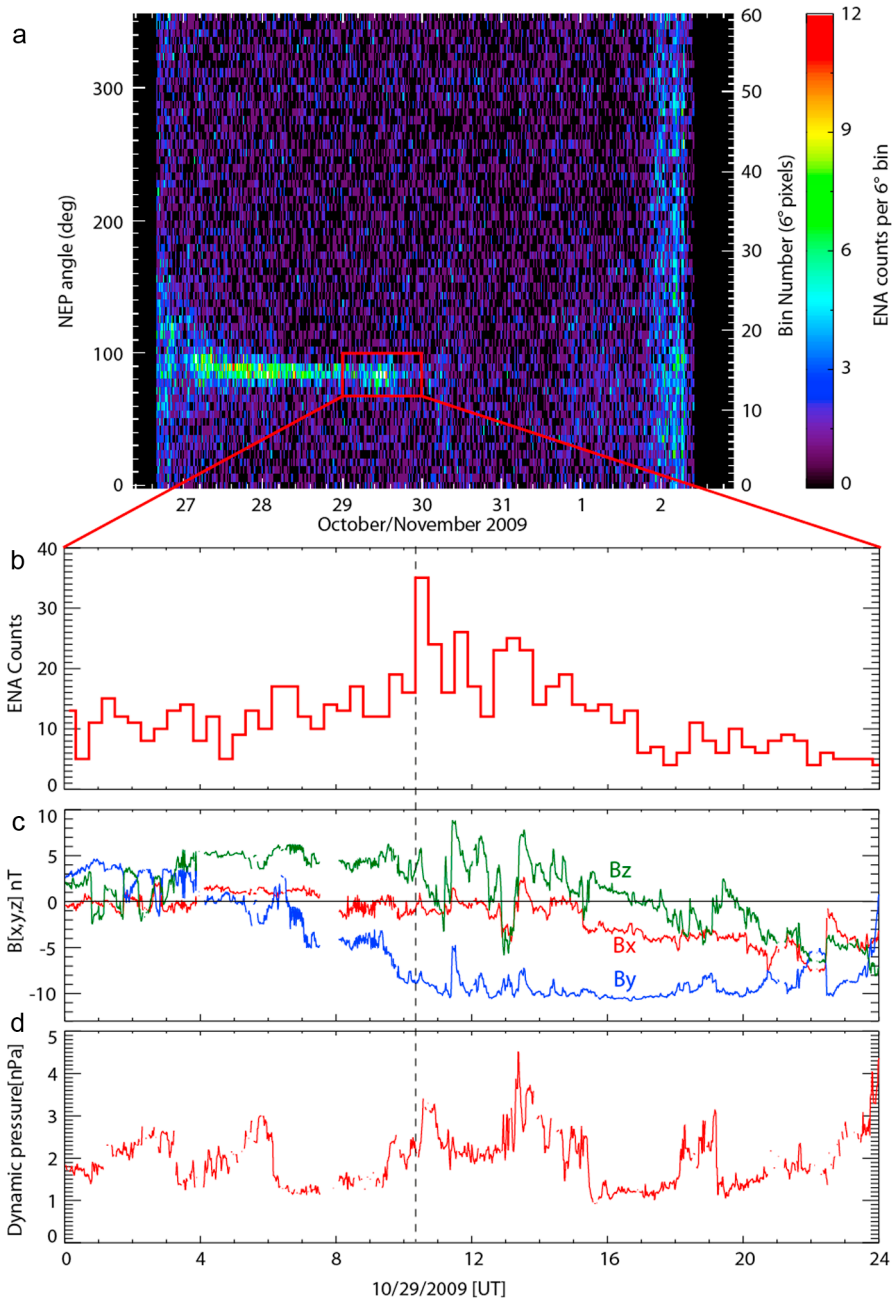

Figure 4. (a) IBEX-Hi energy step 5 (2.0–3.8 keV FWHM) ENA counts for all of IBEX Orbit 51, with the magnetospheric emissions producing the bright band at an NEP angle of ~90°. (b–d) Shown are details from 29 October 2009, when the intensification occurred. Figure 4b gives the integrated counts over 30° in spin phase centered on the magnetotail. Figures 4c and 4d show propagated ACE solar wind parameters for this day.

magnetic dipole from its rotation axis, the plasma sheet flaps up and down over the course of each day. *Hammond et al.* [1994] did a statistical analysis of in situ data to examine the complicated shape and behavior of the plasma sheet and tail boundaries; these authors showed that neutral sheet is highly warped with the largest deflections in the middle of the magnetotail near times of the solstices (these images were made about halfway between equinox and solstice). Finally, since IBEX's orbit carries it from a few R_E above to a few R_E below the equatorial plane, the plasma sheet also appears thicker due to the line of sight not being coplanar with the plasma sheet.

[11] Orbit 51 provides an even more interesting example of the power of IBEX's side-viewing perspective of the magnetosphere. Here the ENA flux, and thus the likely plasma sheet source configuration changes significantly over the time viewed. Figure 3 shows an image of the ENA flux observed by IBEX over the interval from 2121 UT on 27 October 2009 to 1340 UT on 29 October 2009. This interval is indicated by the thicker line segment of the orbit,

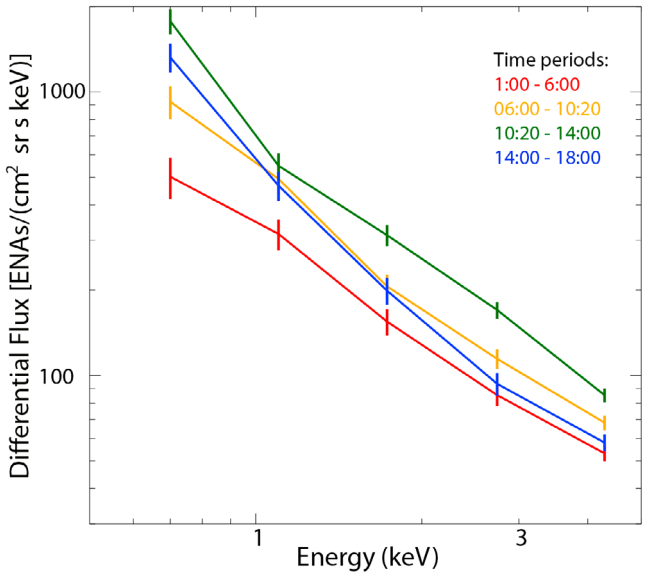

Figure 5. ENA energy spectra for two intervals before (red and yellow) and two intervals after (green and blue) the rapid intensification. Error bars indicate Poisson statistical errors based on the square root of the counts in each sample.

labeled "selected data" in Figure 1, and represents times near apogee when IBEX was ~45 R_E off the side of the Earth and moving very slowly tailward. This image was constructed in GSE coordinates like Figure 2 and uses the same color bar for differential flux. In contrast to Figure 2, however, the highest-ENA fluxes no longer generally follow the model magnetic field, but instead the spatial and temporal variation in the ENA flux are strongly suggestive of a plasma sheet disconnection event occurring somewhere in the inner magnetosphere at ~10 R_E behind the Earth. Here we use the term "plasma sheet disconnection" event rather generally, based on the apparent brightening in ENAs at greater downtail distances. One of the obvious interpretations is that the plasma sheet could have been removed in the form of a plasmoid [e.g., *Hones et al.*, 1984]. Indeed, small flux ropes plasmoids are now known to form frequently as a result of reconnection in the near tail at ~10 R_E [i.e., *Slavin et al.*, 2003] as opposed to the 20–30 R_E distances where reconnection most frequently occurs [*Nagai et al.*, 1998].

[12] Figure 4a shows ENA counts in IBEX-Hi energy step 5 in each 96 spin (~24 min) interval, as a function of angle from the north ecliptic pole (NEP). Vertical brighter bands near the start and end of the orbit are produced by background when the spacecraft was within the magnetosphere. The rest of the orbit is largely quiet with clear magnetospheric emissions at an NEP angle centered at ~90° (prograde in the ecliptic plane). The magnetospheric ENAs drop off over time as IBEX moves slowly tailward, and the emission region viewed maps to progressively greater distances and lower geocoronal densities. However, on 29 October there is a clear intensification of the ENA flux, which indicates an episodic and significant enhancement of ENA emissions from ~10 R_E back in the magnetotail.

[13] The red box in Figure 4a highlights ENAs from the magnetotail (within ±15° centered on the GSE *x* axis) for 29 October; Figures 4b–4d show observations for this day only. Figure 4b provides the total counts in each ~24 min bin. Emissions dropped off to ~10 counts in ESA 5, which corresponds to a triple coincidence rate of ~0.05 Hz. Then at ~1020 UT the ENA flux abruptly rises to 2–3 times its earlier value. There are significant variations in the ENA counts between ~1020 and ~1500, which are much greater than before or after this interval and are larger than expected for Poisson statistics; these variations could indicate further dynamical processes occurring within this region of the tail on much shorter timescales. In fact, the initial intensification is largely contained within a single ~24 min sample, giving a timescale for very enhanced emissions in the IBEX FOV consistent with rapid magnetotail dynamic timescales.

[14] Figures 4c and 4d show ACE SWEPAM and MAG data, which have been shifted to account for the propagation time from ACE at L1 to the magnetopause as a part of the OMNI data set. Figure 4c shows that the abrupt increase in ENA emissions from the tail at ~1020 UT occurred after many hours of northward B_Z and a prolonged (~10 h) rotation of the B_Y from +5 to −10 nT. At the time of the intensification, the solar wind pressure was in the middle of a 2 h increase from ~1.5 to ~3 nPa.

[15] Figure 5 provides the spectral shape of ENA emissions both before and after the intensification shown in Figures 4a and 4b. Starting with the dimmest emissions from 0100–0600 UT (red), the emissions became generally brighter from 0600–1020 UT (yellow), but retain the same spectral shape. Then, the ENA fluxes increased with the intensification (1020–1400), and decayed back to mostly preintensification levels at higher energies (>1 keV) between 1400–1800 UT (blue). The intensification at ~1020 occurred both at lower energies (<1 keV) and higher energies (2–5 keV), with little change around 1 keV. Interestingly, this event shows the simultaneous addition of both hot and cold plasma components with the hot component decaying away while the cold component persists.

3. Discussion

[16] The event observed by IBEX on 29 October is complex and there may be alternate interpretations that could plausibly account for it. However, as visually suggested by Figure 3, the observations may show a plasma sheet disconnection event in the near-tail (roughly −10 R_E) region: possibly in the form of a plasmoid [e.g., *Hones et al.*, 1984] or flux rope [i.e., *Slavin et al.*, 2003]. Throughout the ENA intensification the IMF is extremely benign with northward B_Z and little convection electric field. The 3 h Kp index was no greater than one for the entire first half of the day, and Dst was near zero. All-in-all, this was an extremely quiet day and there was no obvious trigger for the intensification in ENA emissions.

[17] An approximate factor of 2 pressure increase arrived at the magnetopause between ~0930 and 1030 UT, with the intensification coincident with the second half of this increase to within the ENA integration interval (~24 min). This external pressure increase could certainly make the amount of magnetic flux stored in the magnetotail unsustainable and may have driven the magnetotail to shed magnetic flux through a small plasma sheet disconnection event. If this is a near-Earth reconnection event that occurred

within IBEX's FOV, then the spectral information in Figure 5 could be directly showing the particle energization via reconnection across the plasma sheet (the hotter component). In this case, the cooler component might be lower-energy plasma expanding tailward as the plasmoid disconnects and moves down the tail; it is interesting that this cooler plasma enhancement persists after the intensification while the hotter component seems to be associated only with the time of the intensification.

[18] A second possible interpretation of the ENA intensification is adiabatic acceleration of plasma sheet ions due to sudden magnetotail compression caused by an enhancement of solar wind dynamic pressure. *Keika et al.* [2008] showed that the time profile of the total pressure in the plasma sheet is well correlated with that of an impulsive enhancement of the solar wind dynamic pressure. *Miyashita et al.* [2010] reported three tail compression events, which showed an increase in ion temperature and pressure in the plasma sheet. Such adiabatic heating can intensify ENA emissions from the plasma sheet even during otherwise extremely quiet conditions, such as those surrounding this event. Furthermore, the evolution of energy spectra observed here could also be consistent with adiabatic heating/acceleration.

[19] Yet another possible interpretation is that a substorm injection could have occurred deeper in the magnetotail, beyond the distance that IBEX was viewing. Such an event might cause significantly enhanced plasma sheet densities to enter IBEX's FOV from deeper in the tail as the magnetic field becomes more dipolar and plasma sheet material inside the X line is accelerated earthward. However, there is little evidence for an actual substorm in the geomagnetic indices. This event might also be a "pseudobreakup." Such events may involve reconnection and current sheet acceleration, but end before the reconnection reaches lobe field lines. In that case, there might only be partial disconnection, without establishing a significant field aligned current system, consistent with the extremely quiet AE and other indices during this period.

[20] It is interesting to note that the ENA fluxes shown in this study represent geomagnetically quiet times. Large substorms and storms and times of enhanced plasma sheet density should emit significantly more ENAs. For this study we used ~24 min integration times in order to get adequate counting statistics, however, IBEX reports individual ENAs (Direct Events) with extremely high precision (30 s and <0.1° in spin phase), so much higher time resolution of magnetospheric activity can be readily achieved with IBEX when there are adequate ENA fluxes.

[21] In this brief study we have shown the first remote observations of the plasma sheet from outside the magnetosphere. IBEX's near-ecliptic highly elliptical orbit and extremely high-sensitivity ENA cameras provide a truly unique opportunity to study magnetospheric, magnetotail and plasma sheet emissions, morphology, and dynamics from an external, side-viewing vantage point. The IBEX magnetosphere data set is rich with spatial and temporal variations in ENA fluxes and detailed spectral information. Finally, we look forward to collaborative analyses with complimentary magnetospheric ENA observations from TWINS and with a variety of local, in situ measurements from various current and soon-to-be-launched spacecraft (e.g., THEMIS, MMS, RBSP), which should lead to a continuing and bountiful harvest of important new magnetospheric physics results.

[22] **Acknowledgments.** We thank all the outstanding men and women who have made IBEX such a great success and gratefully acknowledge the ACE SWEPAM and MAG Teams as well as the OMNI combined data set. Work at LANL was carried out under the auspices of the U.S. Department of Energy. This research was carried out as a part of the NASA IBEX mission.

[23] Masaki Fujimoto thanks James Slavin and another reviewer for their assistance in evaluating this paper.

References

Bazell, D., E. Roelof, T. Sotirelis, P. Brandt, H. Nair, P. Valek, J. Goldstein, and D. McComas (2010), Comparison of TWINS images of low-altitude emissions (LAE) of energetic neutral atoms (ENA) emissions with DMSP precipitating ion fluxes, *J. Geophys. Res.*, *115*, A10204, doi:10.1029/2010JA015644.

Brandt, P. C., R. Demajistre, E. C. Roelof, S. Ohtani, D. G. Mitchell, and S. Mende (2002), IMAGE/high-energy energetic neutral atom: Global energetic neutral atom imaging of the plasma sheet and ring current during substorms, *J. Geophys. Res.*, *107*(A12), 1454, doi:10.1029/2002JA009307.

Burch, J. L. (2000), IMAGE mission overview, *Space Sci. Rev.*, *91*, 1–14, doi:10.1023/A:1005245323115.

Buzulukova, N., M.-C. Fok, J. Goldstein, P. Valek, D. J. McComas, and P. C. Brandt (2010), Ring current dynamics in modest and strong storms: Comparative analysis of TWINS and IMAGE/HENA data with CRCM, *J. Geophys. Res.*, *115*, A12234, doi:10.1029/2010JA015292.

DeMajistre, R., E. C. Roelof, P. C. Brandt, and D. G. Mitchell (2004), Retrieval of global magnetospheric ion distributions from high energy neutral atom (ENA) measurements by the IMAGE/HENA instrument, *J. Geophys. Res.*, *109*, A04214, doi:10.1029/2003JA010322.

Funsten, H. O., et al. (2009a), Structures and spectral variations of the outer heliosphere in IBEX energetic neutral atom maps, *Science*, *326*, 964–966, doi:10.1126/science.1180927.

Funsten, H. O., et al. (2009b), The Interstellar Boundary Explorer High Energy (IBEX-Hi) neutral atom imager, *Space Sci. Rev.*, *146*, 75–103, doi:10.1007/s11214-009-9504-y.

Fuselier, S. A., et al. (2009), Width and variation of the ENA flux ribbon observed by the Interstellar Boundary Explorer, *Science*, *326*, 962–964, doi:10.1126/science.1180981.

Fuselier, S. A., et al. (2010), Energetic neutral atoms from the Earth's subsolar magnetopause, *Geophys. Res. Lett.*, *37*, L13101, doi:10.1029/2010GL044140.

Grimes, E. W., J. D. Perez, J. Goldstein, D. J. McComas, and P. Valek (2010), Global observations of ring current dynamics during CIR-driven geomagnetic storms in 2008, *J. Geophys. Res.*, *115*, A11207, doi:10.1029/2010JA015409.

Hammond, C. M., M. G. Kivelson, and R. J. Walker (1994), Imaging the effects of dipole tilt on magnetotail boundaries, *J. Geophys. Res.*, *99*(A4), 6079–6092, doi:10.1029/93JA01924.

Henderson, M. G., G. D. Reeves, H. E. Spence, R. B. Sheldon, A. M. Jorgensen, J. B. Blake, and J. F. Fennell (1997), First energetic neutral atom images from Polar CEPPAD/IPS, *Geophys. Res. Lett.*, *24*, 1167, doi:10.1029/97GL01162.

Henderson, M. G., G. D. Reeves, R. Skoug, M. F. Thomsen, M. H. Denton, S. B. Mende, T. J. Immel, P. C:son Brandt, and H. J. Singer (2006), Magnetospheric and auroral activity during the 18 April 2002 saw tooth event, *J. Geophys. Res.*, *111*, A01S90, doi:10.1029/2005JA011111.

Hodges, R. R., Jr. (1994), Monte Carlo simulation of the terrestrial hydrogen exosphere, *J. Geophys. Res.*, *99*(A12), 23,229–23,247, doi:10.1029/94JA02183.

Hones, E. W., Jr., D. N. Baker, S. J. Bame, W. C. Feldman, J. T. Gosling, D. J. McComas, R. D. Zwickl, J. A. Slavin, E. J. Smith, and B. T. Tsurutani (1984), Structure of the magnetotail at 220 Re, *Geophys. Res. Lett.*, *11*, 5–7, doi:10.1029/GL011i001p00005.

Kaufmann, R. L., B. M. Ball, W. R. Paterson, and L. A. Frank (2001), Plasma sheet thickness and electric currents, *J. Geophys. Res.*, *106*, 6179–6193, doi:10.1029/2000JA000284.

Keesee, A., J. Goldstein, D. J. McComas, E. E. Scime, H. Spence, and K. Tallaksen (2011), Remote observations of ion temperatures in the quiet time magnetosphere, *Geophys. Res. Lett.*, doi:10.1029/2010GL045987, in press.

Keika, K., et al. (2008), Response of the inner magnetosphere and the plasma sheet to a sudden impulse, *J. Geophys. Res.*, *113*, A07S35, doi:10.1029/2007JA012763.

McComas, D. J., P. Valek, J. L. Burch, C. J. Pollock, R. M. Skoug, and M. F. Thomsen (2002), Filling and emptying of the plasma sheet: Remote observations with 1–70 keV energetic neutral atoms, *Geophys. Res. Lett.*, *29*(22), 2079, doi:10.1029/2002GL016153.

McComas, D. J., et al. (2009a), The Two Wide-angle Imaging Neutral-atom Spectrometers (TWINS) NASA Mission-of-Opportunity, *Space Sci. Rev.*, *142*, 157–231, doi:10.1007/s11214-008-9467-4.

McComas, D. J., et al. (2009b), IBEX–Interstellar Boundary Explorer, *Space Sci. Rev.*, *146*, 11–33, doi:10.1007/s11214-009-9499-4.

McComas, D. J., et al. (2009c), Global observations of the interstellar interaction from the Interstellar Boundary Explorer (IBEX), *Science*, *326*, 959–962, doi:10.1126/science.1180906.

McComas, D. J., et al. (2009d), Lunar backscatter and neutralization of the solar wind: First observations of neutral atoms from the Moon, *Geophys. Res. Lett.*, *36*, L12104, doi:10.1029/2009GL038794.

Miyashita, Y., K. Keika, K. Liou, S. Machida, Y. Kamide, Y. Miyoshi, Y. Matsumoto, I. Shinohara, Y. Saito, and T. Mukai (2010), Plasma sheet changes caused by sudden enhancements of the solar wind pressure, *J. Geophys. Res.*, *115*, A05214, doi:10.1029/2009JA014617.

Möbius, E., et al. (2009), Direct observations of interstellar H, He, and O by the Interstellar Boundary Explorer, *Science*, *326*, 969–971, doi:10.1126/science.1180971.

Mukai, T., M. Fujimoto, M. Hoshino, S. Kokubun, S. Machida, K. Maezawa, A. Nishida, Y. Saito, T. Terasawa, and T. Yamamoto (1996), Structure and kinetic properties of plasmoids and their boundary regions, *J. Geomagn. Geoelectr.*, *48*, 541–560.

Nagai, T., M. Fujimoto, Y. Saito, S. Machida, T. Terasawa, R. Nakamura, T. Yamamoto, T. Mukai, A. Nishida, and S. Kokubun (1998), Structure and dynamics of magnetic reconnection for substorm onsets with Geotail observations, *J. Geophys. Res.*, *103*(A3), 4419–4440, doi:10.1029/97JA02190.

Nass, H. U., J. H. Zoennchen, G. Lay, and H. J. Fahr (2006), The TWINS-LAD mission: Observations of terrestrial Lyman-alpha fluxes, *Astrophys. Space Sci. Trans.*, *2*, 27–31, doi:10.5194/astra-2-27-2006.

Østgaard, N., S. B. Mende, H. U. Frey, G. R. Gladstone, and H. Lauche (2003), Neutral hydrogen density profiles derived from geocoronal imaging, *J. Geophys. Res.*, *108*(A7), 1300, doi:10.1029/2002JA009749.

Perez, J. D., X.-X. Zhang, P. C. Brandt, D. G. Mitchell, and C. J. Pollock (2004a), Dynamics of ring current ions as obtained from IMAGE HENA & MENA ENA images, *J. Geophys. Res.*, *109*, A05208, doi:10.1029/2003JA010164.

Perez, J. D., X.-X. Zhang, P. C. Brandt, D. G. Mitchell, J.-M. Jahn, C. J. Pollock, and S. B. Mende (2004b), Trapped and precipitating protons in the inner magnetosphere as seen by IMAGE, *J. Geophys. Res.*, *109*, A09202, doi:10.1029/2004JA010421.

Pollock, C. J., et al. (2001), First medium energy neutral atom (MENA) images of Earth's magnetosphere during substorm and storm-time, *Geophys. Res. Lett.*, *28*, 1147–1150, doi:10.1029/2000GL012641.

Pollock, C. J., et al. (2003), The role and contributions of energetic neutral atom (ENA) imaging in magnetospheric substorm research, *Space Sci. Rev.*, *109*, 155–182, doi:10.1023/B:SPAC.0000007518.93331.d5.

Rairden, R. L., L. A. Frank, and J. D. Craven (1986), Geocoronal imaging with Dynamics Explorer, *J. Geophys. Res.*, *91*(A12), 13,613–13,630, doi:10.1029/JA091iA12p13613.

Roelof, E. C. (1987), Energetic neutral atom imaging of a storm-time ring current, *Geophys. Res. Lett.*, *14*, 652–655, doi:10.1029/GL014i006p00652.

Schwadron, N. A., et al. (2009), Comparison of Interstellar Boundary Explorer observations with 3D global heliospheric models, *Science*, *326*, 966–968, doi:10.1126/science.1180986.

Scime, E. E., A. M. Keesee, J.-M. Jahn, J. L. Kline, C. J. Pollock, and M. Thomsen (2002), Remote ion temperature measurements of Earth's magnetosphere: Medium energy neutral atom (MENA) images, *Geophys. Res. Lett.*, *29*(10), 1438, doi:10.1029/2001GL013994.

Skoug, R. M., et al. (2003), Tail dominated storm main phase: 31 March 2001, *J. Geophys. Res.*, *108*(A6), 1259, doi:10.1029/2002JA009705.

Slavin, J. A., E. J. Smith, D. G. Sibeck, D. N. Baker, R. D. Zwickl, and S.-I. Akasofu (1985), An ISEE 3 study of average and substorm conditions in the distant magnetotail, *J. Geophys. Res.*, *90*, 10,875–10,895, doi:10.1029/JA090iA11p10875.

Slavin, J. A., R. P. Lepping, J. Gjerloev, D. H. Fairfield, M. Hesse, C. J. Owen, M. B. Moldwin, T. Nagai, A. Ieda, and T. Mukai (2003), Geotail observations of magnetic flux ropes in the plasma sheet, *J. Geophys. Res.*, *108*(A1), 1015, doi:10.1029/2002JA009557.

Valek, P., P. C. Brandt, N. Buzulukova, M.-C. Fok, J. Goldstein, D. J. McComas, J. D. Perez, E. Roelof, and R. Skoug (2010), Evolution of low altitude and ring current ENA emissions from a moderate magnetospheric storm: Continuous and simultaneous TWINS observations, *J. Geophys. Res.*, *115*, A11209, doi:10.1029/2010JA015429.

Zaniewski, A. M., X. Sun, A. Gripper, E. E. Scime, J.-M. Jahn, and C. J. Pollock (2006), Evolution of remotely measured inner magnetospheric ion temperatures during a geomagnetic storm, *J. Geophys. Res.*, *111*, A10221, doi:10.1029/2006JA011769.

Zoennchen, J. H., U. Nass, G. Lay, and H. J. Fahr (2010), 3D-Geocoronal hydrogen density derived from TWINS Ly-alpha-data, *Ann. Geophys.*, *28*, 1221–1228, doi:10.5194/angeo-28-1221-2010.

M. A. Dayeh, J. Goldstein, J.-M. Jahn, and D. J. McComas, Southwest Research Institute, San Antonio, TX 78228, USA. (dmccomas@swri.org)

H. O. Funsten, Los Alamos National Laboratory, Los Alamos, NM 87545, USA.

S. A. Fuselier and S. M. Petrinec, Lockheed Martin Advanced Technology Center, Palo Alto, CA 94304, USA.

P. Janzen and D. B. Reisenfeld, Department of Physics and Astronomy, University of Montana, Missoula, MT 59812, USA.

D. G. Mitchell, Johns Hopkins University Applied Physics Laboratory, Laurel, MD 20723, USA.

N. A. Schwadron, Department of Physics, University of New Hampshire, Durham, NH 03824, USA.